A&A 444, 947–960 (2005)
DOI: 10.1051/0004-6361:20053806

Astronomy & Astrophysics

The molecular Zeeman effect and diagnostics of solar and stellar magnetic fields

III. Theoretical spectral patterns in the Paschen-Back regime

S. V. Berdyugina[1,2], P. A. Braun[3], D. M. Fluri[1], and S. K. Solanki[4]

[1] Institut für Astronomie, ETHZ, 8092 Zürich, Switzerland
e-mail: sveta@astro.phys.ethz.ch
[2] Astronomy Division, PO Box 3000, 90014 University of Oulu, Finland
[3] Institute of Physics, St.-Petersburg University, Russia
[4] Max-Planck-Institut für Sonnensystemforschung, 37191 Katlenburg-Lindau, Germany

Received 10 July 2005 / Accepted 20 October 2005

ABSTRACT

Many diatomic molecules present in the atmospheres of the Sun and cool stars exhibit the Paschen-Back effect at field strengths typical of sunspots and active cool stars. Here we present a complete theoretical description of the molecular Paschen-Back efect in Hund's cases (a), (b) and all cases intermediate to them. This description allows us to compute the splitting of levels of any multiplicity and the transitions between them. We also introduce a generalized description of the effective magnetic Landé factor applicable not just in the Zeeman regime, but also in the Paschen-Back regime. We find that in the regime of the partial Paschen-Back effect strongly asymmetric Stokes profiles are produced, whose strengths and asymmetries depend sensitively on the magnetic field. In the regime of the complete Paschen-Back effect the profiles become symmetric again (although they may be strongly shifted). The strength of the forbidden and satellite transitions increases rapidly with field strength in the partial Paschen-Back regime, while the strength of the main branch transitions decreases. These signatures hold promise to form the basis of new diagnostics of solar and stellar magnetic fields.

Key words. magnetic fields – molecular processes – polarization – Sun: magnetic fields – stars: magnetic fields

1. Introduction

This is the third in a series of papers aimig at a systematic study of the molecular Zeeman effect and its diagnostic capabilities for measuring magnetic fields on the Sun and cool stars. In our first paper (Berdyugina & Solanki 2002, hereafter Paper I), we presented an overview of the theory of the Zeeman effect in diatomic molecules for the limiting Hund's cases (a) and (b) and developed a numerical approach for the intermediate coupling case (a, b) which is valid for terms of any multiplicity. We also deduced general properties of the Zeeman splitting in molecular lines and calculated Landé factors for prominent molecular bands in sunspot and cool-star spectra. In the second part (Berdyugina et al. 2003, hereafter Paper II), we described the Stokes radiative transfer of Zeeman split molecular lines and computed Stokes profiles of those transitions previously studied in Paper I that represent important diagnostics of sunspot and starspot magnetic fields.

Thanks to the recent theoretical developments, molecular spectropolarimetry becomes a rapidly developing field in astrophysics. The first successful calculation of molecular Stokes profiles and comparison with observations (TiO and MgH transitions in sunspots) was presented by Berdyugina et al. (2000). Peculiar Stokes profiles of CN and OH transtions observed in sunspots were modelled and explained by Berdyugina et al. (2001), Berdyugina & Solanki (2001) and Asensio Ramos et al. (2005). A study of the Zeeman effect in the G-band CH transitions was carried out by Uitenbroek et al. (2004) and Asensio Ramos et al. (2004).

In the present paper we extend our theoretical investigation started in Paper I to the Paschen-Back regime (PBR), i.e. when the perturbation due to an external magnetic field becomes comparable with internal interactions in the molecule. The Paschen-Back effect plays a much more dominant role for diatomic molecular transitions than for their atomic counterparts, since energy levels in molecules are closer to each other due to, e.g., rotational or multiplet splitting. In such a case the Paschen-Back regime is reached for lower field strengths than typically found on the Sun and other cool stars (Paper I).

A theory of the molecular Zeeman effect in the Paschen-Back regime was first considered by Hill (1929), who described splitting of molecular doublet levels for the intermediate case (a, b) using the Hund's case (b) wavefunctions. He did not succeed though in calculations of theoretical line

strengths for this case. The latter problem was resolved much later by Schadee (1978), who repeated the analytical calculation by Hill using the Hund's case (a) wavefunctions. He did not give details on line strength calculations, however, as the corresponding analytical expressions would be too complicated. Both above approaches were limited to doublet states and for the Paschen-Back effect (PBE) on the fine structure of molecular levels, i.e. when spin becomes uncoupled from other momenta by an external magnetic field.

Here we present a more general numerical approach to the molecular PBE which is valid for terms of any multiplicity and accounts for interactions of all rotational levels in a molecule. In Sect. 2 we introduce the magnetic perturbation on the molecular Hamiltonian and explain how the theoretical line strengths are computed in the PBR. We also define a generalized effective Landé factor which is applicable in both the Zeeman and Paschen-Back regimes. In Sect. 3 we present calculations of molecular levels and of different multiplicity in the PBR when the magnetic splitting becomes comparable with the fine structure. This is further extended for the rotational structure in Sect. 4. Pecularities of the transitions between magnetic sublevels in the Paschen-Back regime and their Stokes profiles are discussed in Sect. 5. We summarize our results and conclusions in Sect. 6.

2. Magnetic perturbation of the molecular Hamiltonian

2.1. Energy levels

In the presence of a magnetic field the Hamiltonian of a molecule in an intermediate coupling case is described by the sum of the internal interaction energies and the magnetic energy:

$$\mathcal{H} = \mathcal{H}_{\rm int} + \mathcal{H}_{\rm H}. \quad (1)$$

Here the main contribution to the internal energy $\mathcal{H}_{\rm int}$ is due to the spin-orbital $\mathcal{H}_{\rm SL}$ and rotational $\mathcal{H}_{\rm rot}$ energies. The energies due to spin-rotation $\mathcal{H}_{\rm SR}$, orbit-rotation $\mathcal{H}_{\rm LR}$, spin-spin $\mathcal{H}_{\rm SS}$ and other interactions as well as the correction due to centrifugal distortion $\mathcal{H}_{\rm c}$ can be added:

$$\mathcal{H}_{\rm int} = \mathcal{H}_{\rm SL} + \mathcal{H}_{\rm rot} + \mathcal{H}_{\rm c} + \mathcal{H}_{\rm SR} + \mathcal{H}_{\rm LR} + \mathcal{H}_{\rm SS} + \ldots \quad (2)$$

In the present paper we limit ourselves to interactions within one electronic state. The Zeeman and Paschen-Back effects for interacting electronic states is the subject of a forthcoming paper. The energy of the interaction of the molecular magnetic moment μ with the external magnetic field $\boldsymbol{H}$ is a scalar product of the two vectors:

$$\mathcal{H}_{\rm H} = \mu \cdot \boldsymbol{H} = \mu_0(\boldsymbol{L} + 2\boldsymbol{S}) \cdot \boldsymbol{H}, \quad (3)$$

where μ_0 is the Bohr magneton, $\boldsymbol{S}$ is the spin, and $\boldsymbol{L}$ is the orbital momentum. If the magnetic moments due to spin and orbital motion of electrons are zero, the contributions from the rotation and spins of nuclei need to be taken into account.

In the Zeeman regime, when the internal coupling of the momenta is larger than the interaction with the external magnetic field, the diagonalisation of the internal Hamiltonian can be first performed, while the interaction with the magnetic field can be treated as a perturbation. This approach has been developed in Paper I and applied to many astrophysical molecules (see also Paper II).

In the strong-field regime, a transition to the Paschen-Back effect occurs, i.e. the magnetic interaction becomes comparable to or even larger than the internal interactions. Then, the diagonalisation of the full Hamiltonian given by Eq. (1) should be performed. For an increasing magnetic field strength, the PBE will first occur on neighbouring interacting levels and then on the whole level structure.

The full Hamiltonian $\mathcal{H}$ can be expressed in both Hund's case (a) and (b) wavefunctions. The choice can be made depending on a particular transition. Matrix elements of the internal Hamiltonian $\mathcal{H}_{\rm int}$ in the basis of the Hund's case (a) and (b) wavefunctions are given in Tables A.1 and A.2, respectively, according to Kovàcs (1969). In the tables, A, B, D, γ and λ denote constants of spin-orbital coupling, rotational splitting, centrifugal distortion, spin-rotational and spin-spin coupling, respectively. Molecular quantum numbers have their conventional meaning. Matrix elements of the magnetic perturbation $\mathcal{H}_{\rm H}$ expressed in the basis of the Hund's case (a) wavefunctions are given in Table A.3, according to Schadee (1978), but with a correction to match the sign convention for the spin operator by Kovàcs (1969). In Table A.4 corresponding magnetic matrix elements are given for the Hund's case (b) wavefunctions, according to Hill (1929). In these tables, $\Delta\sigma_0 = \mu_0 H$, where H is the magnetic field strength.

Non-zero elements of the perturbation matrix indicate pairs of levels interacting with each other. As the magnetic field strength increases, the values of such elements also increase, indicating that the levels approach each other in energy. Mixing of levels occurs however in such a way that interacting levels cannot intersect. Instead, the levels experience "repulsion", i.e. the higher level is displaced upward and the lower level downward. In addition, since wavefunctions become mixed, each of the interacting levels assumes properties of the other. As seen from Table A.3, the selection rules for the interacting levels within the same electronic state described in the Hund's case (a) wavefunctions are as follows: $\Delta M = 0$, $\Delta J = 0, \pm 1$, and $\Delta\Sigma = 0, \pm 1$. In the Hund's case (b) wavefunctions, the same rules hold (as seen from Table A.4) with the latter condition being replaced by $\Delta N = 0, \pm 1$.

Eigenvalues of the full Hamiltonian $\mathcal{H}$ represent magnetic sublevels of a molecule in a given electronic state for the intermediate Hund's case (a, b) in the PBR. Corresponding eigenvectors define new wavefunctions $\Psi^{\rm H}$ as linear combinations of the basis wavefunction Ψ^a or Ψ^b:

$$\Psi^{\rm H}_M = \sum_{\Sigma,J} C^a_{\Sigma JM}\Psi^a_{\Sigma JM} = \sum_{N,J} C^b_{NJM}\Psi^b_{NJM}. \quad (4)$$

A number of mixing basis wavefunctions depend on the strength of the magnetic field. If only levels with different spin projections are mixed, the PBE occurs on the fine structure. This was previously analytically described by Hill (1929) and Schadee (1978) for doublet states. In Sect. 3 we present results of our numerical calculations for doublet, triplet and quartet

states with various spin coupling constants. If levels with different J in case (a) or N in case (b) are mixed, the PBE occurs on the rotational structure. Both Hill and Schadee neglected this interaction for the sake of simplicity. When carrying out numerical diagonalisation of the Hamiltonian, this interaction can be easily taken into account. This is the subject of our discussion in Sect. 4.

2.2. Transition probabilities

Strengths of transitions between Zeeman sublevels are expressed via matrix elements of the electric dipole operator $\mu_{\rm e}$. Generally, the transition probability is a product of the square of the electronic transition moment, the Franck-Condon factor and the Hönl-London factor (HLF). Leaving out the first two factors, one can determine the magnetic Hönl-London factor as the square of the matrix element of the electric dipole operator in the new wavefunctions:

$$\begin{aligned}\mathcal{S}^{\rm H}_{M''M'} &= \left|\left\langle \Psi^{\rm H}_{M''}|\mu_{\rm e}|\Psi^{\rm H}_{M'}\right\rangle\right|^2 \qquad (5)\\ &= \left|\left\langle \sum_{\Sigma''J''} C^a_{\Sigma''J''M''}\Psi^a|\mu_{\rm e}|\sum_{\Sigma'J'} C^a_{\Sigma'J'M'}\Psi^a\right\rangle\right|^2\\ &= \left|\left\langle \sum_{N''J''} C^b_{N''J''M''}\Psi^b|\mu_{\rm e}|\sum_{N'J'} C^b_{N'J'M'}\Psi^b\right\rangle\right|^2.\end{aligned}$$

Here the single and double primes correspond to the upper and lower level, respectively. To make the equation more compact we neglected subscripts for the wavefunctions. The subscripts are the same as for corresponding eigenvectors. The new amplitude of the transition $\langle\Psi^{\rm H}_{M''}|\mu_{\rm e}|\Psi^{\rm H}_{M'}\rangle$ is thus a specific sum of the transition amplitudes in the basis wavefunctions, either case (a) $\langle\Psi^a_{\Sigma''J''M''}|\mu_{\rm e}|\Psi^a_{\Sigma'J'M'}\rangle$ or case (b) $\langle\Psi^b_{N''J''M''}|\mu_{\rm e}|\Psi^b_{N'J'M'}\rangle$. The matrix elements of the electric dipole operator in Hund's case (a) are well known expressions (e.g., Hougen 1970; Schadee 1978). In terms of the rotation group they can be presented in a general form (cf., Berdyugina et al. 2002).

In the Hund's case (a) wavefunctions the unperturbed transition amplitude is as follows:

$$\begin{aligned}\left\langle\Psi^a_{\Sigma''J''M''}|\mu_{\rm e}|\Psi^a_{\Sigma'J'M'}\right\rangle &= (-1)^{J'+M''+1}\sqrt{2J''+1}\begin{pmatrix}J' & J'' & 1\\ -M' & M'' & -\Delta M\end{pmatrix}\\ &\times(-1)^{J'+\Omega''+1}\sqrt{2J'+1}\begin{pmatrix}J'' & J' & 1\\ -\Omega'' & \Omega' & -\Delta\Omega\end{pmatrix}. \qquad (6)\end{aligned}$$

Here, the first term describes the dependence of transition amplitudes on J and M, while the second one is a reduced matrix element providing the dependence on Ω.

In the Hund's case (b) wavefunctions the expression for the unperturbed transition amplitude is as follows:

$$\begin{aligned}&\langle\Psi^b_{N''J''M''}|\mu_{\rm e}|\Psi^b_{N'J'M'}\rangle =\\ &\quad(-1)^{J'+M''+1}\sqrt{2J''+1}\begin{pmatrix}J' & J'' & 1\\ -M' & M'' & -\Delta M\end{pmatrix}\\ &\quad\times(-1)^{N''+S+J'+1}\sqrt{2J'+1}\sqrt{2N''+1}\begin{Bmatrix}N'' & N' & 1\\ J' & J'' & S\end{Bmatrix}\\ &\quad\times(-1)^{N'+\Lambda''+1}\sqrt{2N'+1}\begin{pmatrix}N'' & N' & 1\\ -\Lambda'' & \Lambda' & -\Delta\Lambda\end{pmatrix}. \qquad (7)\end{aligned}$$

Here the first term is the same as in Eq. (6). The second term arises due to the vector sum of $\boldsymbol{S}$ and $\boldsymbol{N}$. The third term is the reduced matrix element providing the dependence on Λ. In the Zeeman regime the first term remains unchanged also for the intermediate Hund's case (a, b), as was shown in Paper I. This implies that in the weak field regime the total line strength depends on the perturbation due to spin uncoupling, while relative intensities of the Zeeman components are preserved. In the strong field regime, the Paschen-Back effect results in alteration of both the total line strength and relative intensities of the Zeeman components.

2.3. Landé factors

Knowing shifts and strengths of Zeeman transitions, one can calculate the effective Landé factor of a given spectral line. In the Zeeman regime, it is defined as follows:

$$g_{\rm eff} = \sum_{M''}\widetilde{\mathcal{S}}_{M'M''}(g'M' - g''M''), \qquad (8)$$

where g' and g'' are Landé factors of the upper and lower level, respectively, and the sum should be calculated only for $\Delta M = 1$. The strengths of Zeeman transitions $\widetilde{\mathcal{S}}_{M'M''}$ are normalised as follows:

$$\sum_{\Delta M=k}\widetilde{\mathcal{S}}_{M'M''} = 1, \qquad k = +1, 0, -1. \qquad (9)$$

We can further obtain expressions for the effective Landé factors of the transitions belonging to three rotational branches R, Q and P ($\Delta J = 1,\ 0,\ -1$, respectively):

$$\begin{aligned}g_{\rm eff}(R) &= \frac{1}{2}[g'(J'+1) - g''J''],\\ g_{\rm eff}(P) &= \frac{1}{2}[-g'J' + g''(J''+1)],\\ g_{\rm eff}(Q) &= \frac{1}{2}[g' + g'']. \qquad (10)\end{aligned}$$

Note that these formulae differ from the corresponding ones in Paper I by the factor 1/2, because of the different definition of the effective Landé factor used in Paper I, where it represented the mean weighted difference between transitions with $\Delta M = +1$ and -1 (so-called σ^+ and σ^- components). Here we use the conventional definition that it is the mean weighted shift of one of the sigma transitions with respect to the zero-field position.

The effective Landé factors are useful for the so-called weak-field approximation, when the magnetic splitting is smaller than the spectral line width broadened by other processes. For most molecular transitions under solar conditions this approximation is acceptable. However, the above definition is only useful in the Zeeman regime, when the magnetic splitting is symmetrical and Landé factors of levels are independent of magnetic field strength (see Paper I).

In the case of the PBE, the weak-field approximation can still hold for almost all molecular transitions involving Σ states at moderate field strengths. However, the splitting is no longer symmetrical and line strengths are modified due to the magnetic interaction. We suggest therefore a generalised definition of the effective Landé factor. First, we define the partial

strengths of the σ^+, σ^- and π components corresponding to $\Delta M = +1, -1, 0$ as follows:

$$\mathcal{S}^+ = \sum_{\Delta M=+1} \mathcal{S}^{\rm H}_{M'M''}, \tag{11}$$

$$\mathcal{S}^- = \sum_{\Delta M=-1} \mathcal{S}^{\rm H}_{M'M''}, \tag{12}$$

$$\mathcal{S}^0 = \sum_{\Delta M=0} \mathcal{S}^{\rm H}_{M'M''}. \tag{13}$$

Then, we define the effective Landé factors for σ^+, σ^- and π components:

$$g^+ = \frac{1}{\mu_0 H} \sum_{M'',\Delta M=+1} \frac{\mathcal{S}^{\rm H}_{M'M''}}{\mathcal{S}^+}(\Delta E' - \Delta E''), \tag{14}$$

$$g^- = \frac{1}{\mu_0 H} \sum_{M'',\Delta M=-1} \frac{\mathcal{S}^{\rm H}_{M'M''}}{\mathcal{S}^-}(\Delta E' - \Delta E''), \tag{15}$$

$$g^0 = \frac{1}{\mu_0 H} \sum_{M'',\Delta M=0} \frac{\mathcal{S}^{\rm H}_{M'M''}}{\mathcal{S}^0}(\Delta E' - \Delta E''), \tag{16}$$

where ΔE is the energy shift for a given magnetic sublevel. Finally, we can define the effective Landé factor in the PBR:

$$g_{\rm eff} = \frac{1}{2}(g^+ - g^-). \tag{17}$$

It is easy to see that in the Zeeman regime $g^+ = -g^-$, and the above definition coincides with the conventional one. In the following we use the above new definitions for studying deviations from the Zeeman regime.

3. Paschen-Back effect on the fine structure

3.1. Intermediate Paschen-Back regime

In this section we consider the PBE on the fine structure, when only levels with different spin projections are mixed. For doublet states with weak spin coupling this was previously analytically described by Hill (1929) and Schadee (1978) and discussed in detail by Illing (1981). Our numerical calculations reproduce exactly the examples calculated by Schadee and Illing for doublet transitions of MgH and CN. In this section, in addition to doublet states, we present examples of our numerical calculations for triplet and quartet states with the projection of the orbital angular momentum on the internuclear axis $\Lambda = 0, 1, 2$, i.e. Σ, Π and Δ states.

The behaviour of the electronic states in a magnetic field depends on how strongly the electron spin is coupled to the internuclear axis and the orbital moment. In case when $\Lambda = 0$ the spin is completely uncoupled from the internuclear axis (spin-orbital interaction constant $A = 0$) and only weakly coupled to the rotation (spin-rotation interaction constant $\gamma \ll 1$). This implies that even a very weak magnetic field can significantly perturb the fine structure of molecular levels. This effect is demonstrated for $^2\Sigma$, $^3\Sigma$ and $^4\Sigma$ states in Fig. 1. The level structure becomes significantly perturbed when the magnetic splitting $\mu_0 H$ becomes comparable to the fine structure splitting γN. If γ is of the order of 10^{-2}, the perturbation becomes noticeable at field strengths well below 1 kG.

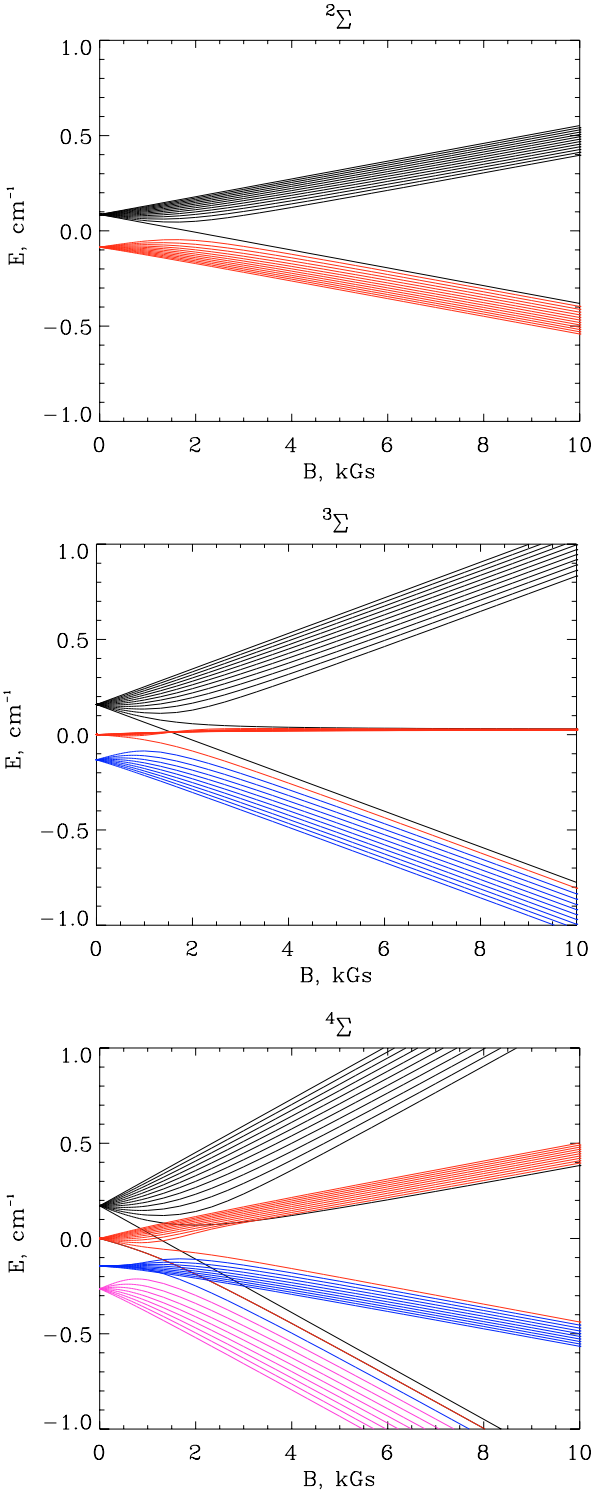

Fig. 1. The PBE effect on the fine structure of $^2\Sigma$,$^3\Sigma$ and $^4\Sigma$ states for $N = 6, 5, 4$, respectively. The spin-rotational interaction constant γ is 0.026 cm^{-1} and the rotational constant B is 5.736463 cm^{-1}. The transition to the PBR occurs at field strengths below 1 kG. The complete PBE in the $^2\Sigma$ state occurs at about 2 kG, in $^3\Sigma$ and $^4\Sigma$ at about 3 kG.

In case when $\Lambda \neq 0$, the fine structure is defined by the spin-orbital interaction. Examples of the level splitting for $^2\Pi$, $^3\Pi$ and $^4\Delta$ are shown in Fig. 2. Here the field strength at which the PBE becomes significant is defined by the spin-orbital interaction constant A: the magnetic splitting $\mu_0 H$ should be of the order of $A\Lambda$. For $A \sim 1{-}10$ the transition to the PBR occurs at few kG fields.

3.2. Complete Paschen-Back effect on the fine structure

When the spin is completely uncoupled from both the internuclear axis and the rotation, the complete Paschen-Back effect on the fine structure occurs. The spin and the angular momentum $\boldsymbol{N}$ are independently quantised in the field direction with component M_S and M_N. The splitting in this case is described by the known asymptotic expression (e.g., Herzberg 1950):

$$\Delta E = \mu_0 H \left[\frac{\Lambda^2 M_N}{N(N+1)} + 2M_S \right]. \quad (18)$$

This formula is valid as long as the Zeeman splitting is large compared to the multiplet splitting but still smaller than the rotational splitting. Note that the first term is of the same form as for the singlet transitions in Hund's case (a) (see Paper I). The first term decreases rapidly as N increases, whereas the second term is independent of N. For higher N there is practically only a splitting into components corresponding to $M_S = -S, -S+1, ..., S$, with a separation of $\mu_0 H$. For Σ states, when $\Lambda = 0$, the first term is zero, and there remains only a splitting independent of N. A more detailed calculation, when the spin-rotation interaction is taken into account, reveals that each component with a given M_S splits into $2N+1$ components with splitting of the same order of magnitude as the multiplet splitting without magnetic field. The level splitting in the complete PBR is thus reminiscent of the multiplet structure. This is clearly visible in Figs. 1 and 4 for Σ states at moderately strong fields and in Fig. 2 for states with $\Lambda \neq 0$ at stronger fields.

4. Paschen-Back effect on the rotational structure

In this section we consider the PBE on the rotational structure, when levels with different J in case (a) or N in case (b) are mixed. This interaction has not been discussed in detail so far.

4.1. States closer to Hund's case (a)

In this case, the electronic angular momenta are strongly coupled to the line joining the nuclei and only weakly with the rotation of nuclei. The electronic term structure is characterised by larger multiplet splitting compared to the rotational splitting. When magnetic shifts become comparable with the rotational splitting, levels corresponding to the same M numbers and $\Delta J = \pm 1$ start to interact. This is illustrated in Fig. 3 for a $^2\Pi_{3/2}$ state with strong spin-rotational interaction. The repulsion of levels with $\Delta J = \pm 1$ becomes significant when magnetic splitting become comparable to rotional one, i.e. $\mu_0 H \sim 2B(J+1)$. In this example, the second state in the doublet, $^2\Pi_{1/2}$, is separated by about 100 cm^{-1} and remains magnetically insensitive, in accord with Hund's case (a).

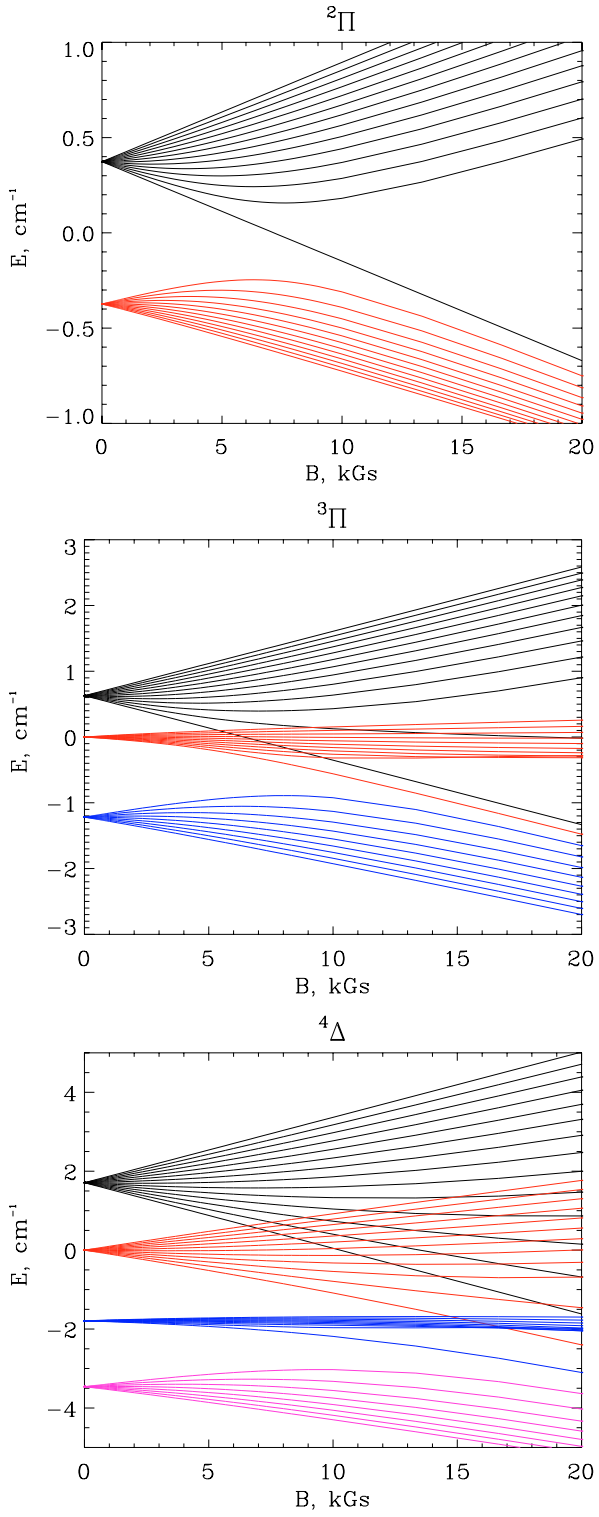

Fig. 2. The PBE effect on the fine structure of $^2\Pi$, $^3\Pi$ and $^4\Delta$ states for $N = 6, 5, 4$, respectively. The spin-orbital interaction constant A is 12 cm^{-1} for the Π states and 3 cm^{-1} for the Δ state. The rotational constant B is 5 cm^{-1} and 3 cm^{-1}, correspondingly. The transition to the PBR occurs at field strengths of a few kG. The complete PBE in the $^2\Pi$ state occurs at about 10 kG, in $^3\Pi$ at 15 kG and in $^4\Delta$ at about 30 kG.

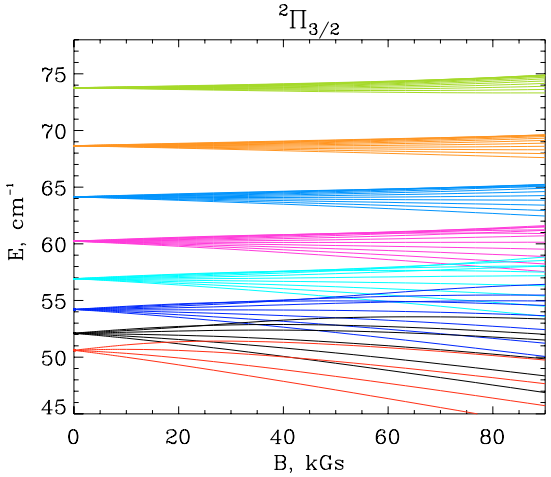

Fig. 3. The PBE effect on the rotational structure of a $^2\Pi_{3/2}$ state in Hund's case (a) for J from 1.5 to 8.5. The spin-orbital interaction constant A is 100 cm^{-1}, and the rotational constant B is 0.3 cm^{-1}. The PBE is significant already at 15 kG field strengths, when $\mu_0 H \sim 2B(J+1)$.

The interaction of the two substate becomes significant only at very large field strengths. Then, the PBE occurs on the fine structure as well. A similar behaviour is found for other states with $\Lambda \neq 0$ and $S \neq 0$. Note that rotational levels of singlet states do not perturb each other and split according to the conventional Zeeman effect, unless perturbations due to other electronic states are significant and should be taken into account.

4.2. States closer to Hund's case (b)

In this case, the spin is only weakly coupled to the internuclear axis, orbital momentum and the rotation of nuclei. The electronic term structure is characterised by larger rotational splitting compared to the multiplet splitting. As discussed above, for an increasing magnetic field strength, the PBE occurs first at the fine structure, i.e. levels with the same M and N numbers and $J = \pm 1$ start to interact. When magnetic shifts exceed the multiplet splitting and become comparable with the rotational splitting, levels with $N = \pm 1$ start to interact. This is illustrated in Fig. 5 for states with $\Lambda \neq 0$. The increasing magnetic splitting and the repulsion of interacting levels lead to complete smearing of the rotational and multiplet structure, indicating the complete PBE within a given electronic state.

A special case represents states with $\Lambda = 0$, i.e. Σ states. As shown in Fig. 4, the rotational structure of such states is not further perturbed by an increasing magnetic field. The pseudo-multiplet structure of the levels resulting from the complete PBE on the fine structure is conserved over a wide range of magnetic field strengths. Only additional perturbations by other electronic states would change this picture.

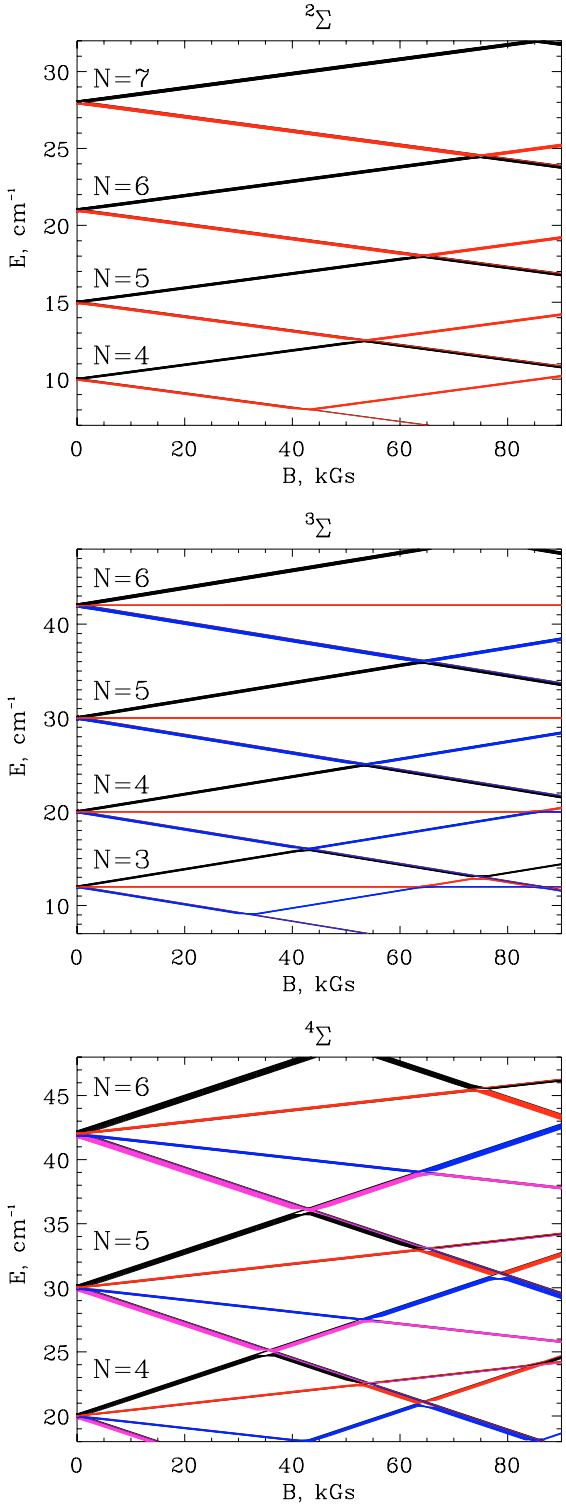

Fig. 4. The PBE effect on the rotational and fine structure of $^2\Sigma$, $^3\Sigma$ and $^4\Sigma$ states. The spin-rotational interaction constant γ is 0.026 cm^{-1}. The rotational constant B is 0.5 cm^{-1} for the $^2\Sigma$ state and 1 cm^{-1} for the others. The complete PBE occurs at a few kG field strengths. The levels with different N numbers are not interacting and can intersect as the splitting increases.

5. Transitions in the Paschen-Back regime

5.1. Magnetic patterns

Selection rules for electric dipole transitions in pure Hund's cases (a) and (b) are immediately seen from Eqs. (6) and (7). In the case (a), only those transition amplitudes are not zero for which $\Delta\Omega = 0, \pm 1$, $\Delta\Lambda = 0, \pm 1$, $\Delta\Sigma = 0$, $\Delta J = 0, \pm 1$, $\Delta M = 0, \pm 1$, with $\Delta J = 0$ being forbidden for $\Omega = 0 \rightarrow \Omega = 0$ transitions. In the case (b), Ω and Σ are not defined, and the

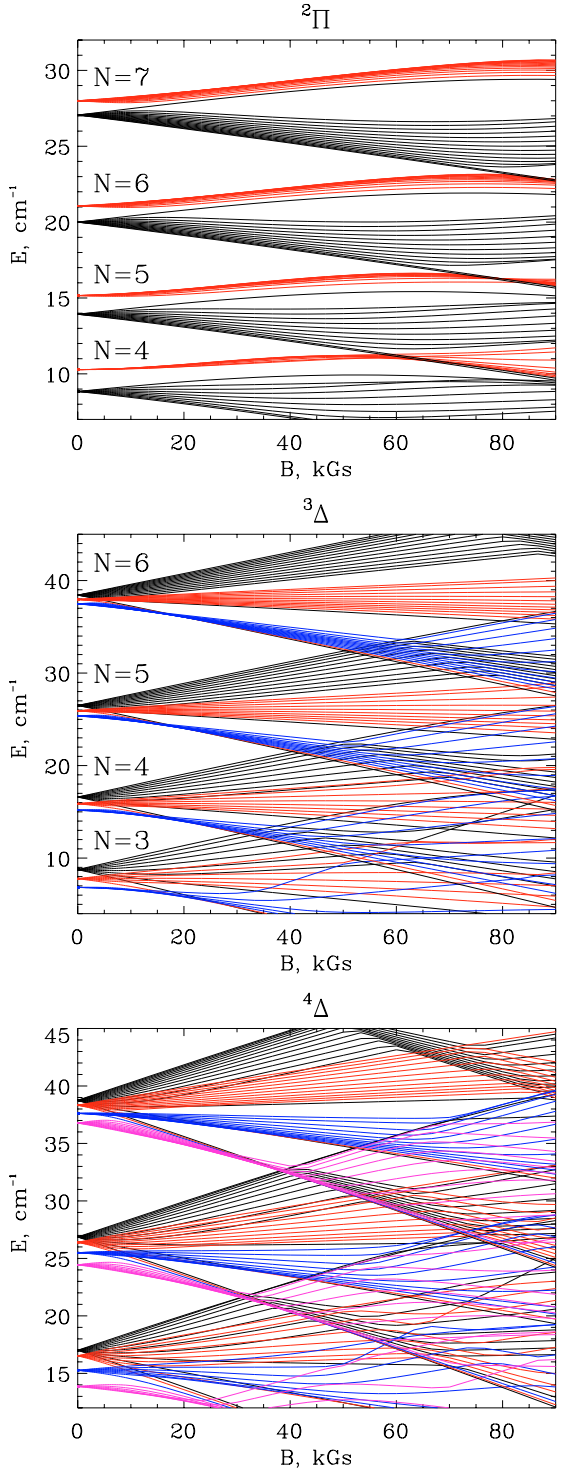

Fig. 5. The PBE effect on the rotational and fine structure of $^2\Pi$, $^3\Delta$ and $^4\Delta$ states. The spin-orbital interaction constant A is 5 cm^{-1} for the $^2\Pi$ state, 1 cm^{-1} for the $^3\Delta$ state and 3 cm^{-1} for the $^3\Delta$ state. The rotational constant B is 0.5 cm^{-1} for the $^2\Pi$ state and 1 cm^{-1} for the Δ states. The complete PBE on the fine structure occurs at field strengths of a few kG. As the splitting increases, the levels with different N mix with each other. The interacting levels cannot intersect and deviate from the normal Zeeman splitting.

selection rules for them are replaced by those for ΔN and ΔS: $\Delta\Lambda = 0, \pm1, \Delta S = 0, \Delta N = 0, \pm1$, $\Delta J = 0, \pm1$, $\Delta M = 0, \pm1$ with $\Delta N = 0$ being forbidden for $\Lambda = 0 \rightarrow \Lambda = 0$ transitions. In case of weak magnetic perturbation (Zeeman regime) the electric dipole selection rules for the case intermediate between Hund's case (a) and (b) allow the same transitions as in the case (b). If $\Delta J = \Delta N$, then the rotational branches R, P and Q with $\Delta J = +1, -1, 0$, respectively, are called main. If $\Delta J \neq \Delta N$, satellite branches appear, e.g. ${}^PR, {}^Q P$, etc., where the left superscript denotes the branch type according to the value of ΔN.

Strong magnetic perturbation in the PBR, as considered in the present paper, results in mixing levels with different N, J and S. These quantum numbers loose therefore their identity. In this case the only good quantum numbers left are Λ and M. Thus, the selection rules for the intermediate Hund's case (a, b) in the PBR are $\Delta\Lambda = 0, \pm1$ and $\Delta M = 0, \pm1$. This implies that many transitions that are forbidden in the Zeeman regime become allowed in the PBR. For instance, transitions with $\Delta J = \pm2$ corresponding to the rotational branches S (do not confuse with spin) and O become stronger as the field increases. Also, previously allowed but weak transitions in satellite branches increase in strength.

The appearance of previously forbidden transitions and strengthening of satellite transitions are compensated by reduced amplitudes of the allowed transitions. Thus, as the strength of magnetic field increases and the level structure enters the PBR, main branch transitions start to fade while giving the power to forbidden and satellite transitions. This is illustrated in Fig. 6 for the MgH $A^2\Pi - X^2\Sigma^+$ system. Along with the change of the total line strength, the intensity of the $\Delta M = +1, 0, -1$ transitions varies in different ways, so that the line is no longer symmetric. This results in different partial strengths of the σ^+, σ^- and π components. In other words, the radiative properties of a molecule become dependent on the magnetic field, which results in so-called molecular magnetic dichroism. This is a typical behaviour of all molecular transitions in strong magnetic fields.

The asymmetry between the strengths of the line Zeeman component is accompanied by the asymmetry in its Landé factors. This is illustrated in Fig. 7, where variations of $g_{\rm eff}$, g^+, g^0 and g^- are shown. In the Zeeman regime Landé factors of the main branch lines are relatively small (see Paper I), while satellite transitions are very magnetically sensitive but weak. As the magnetic field strength increases, all lines show significant magnetic sensitivity, especially satellite and forbidden transitions. The most rapid changes occur in the intermediate PBR. In this case large polarisation signals are expected from all lines. When the Landé factors are combined with the line strengths, the satellite and forbidden transitions would significantly contribute to the polarisation signal in the PBR. When both upper and lower states approach the complete PBR on the fine structure, the splitting and partial strengths of different Zeeman components become symmetric again. Similar behaviour is expected for all other molecular electronic transitions.

Magnetic patterns of the discussed transitions at four different field strengths of 0.1, 1, 10 and 100 kG are shown in Figs. 8 and 9. These examples demonstrate the complex behaviour of line strengths and splitting when only the lower state is in the

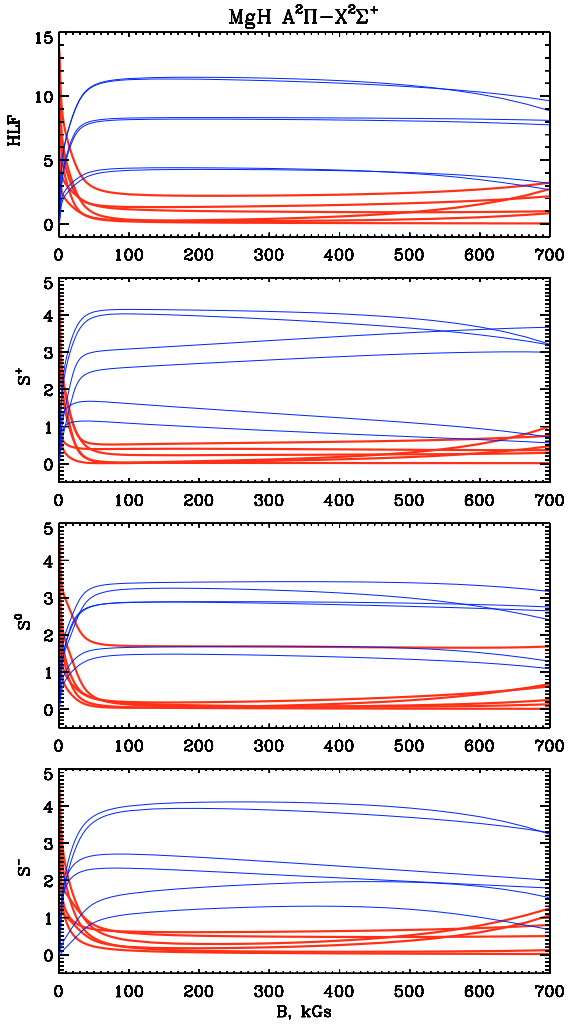

Fig. 6. Hönl-London factors (HLF) and partial strengths of the σ^+, σ^- and π components ($\mathcal{S}^+$, $\mathcal{S}^0$ and $\mathcal{S}^-$) for six main branch transitions (thick lines) and six satellite transitions (thin lines) with $N'' = 6$ in the MgH $A^2\Pi - X^2\Sigma^+$ system. Strengths of the satellite transition with $\Delta J = 0, \pm 1$ in the non-magnetic case are very small and those of the forbidden transitions with $\Delta J = \pm 2$ are zero. As the magnetic field strength increases, lines of the main branches fade, while the satellite and forbidden transitions increase in power. The most rapid changes occur in the intermediate PBR. The structure is stabilised when both upper and lower electronic states are in the complete PBR on the fine structure. When the PBE starts to influence the rotational molecular structure, some main branch lines become stronger again, while satellite and forbidden transitions weaken. Such a behaviour is typical for other electronic transitions as well.

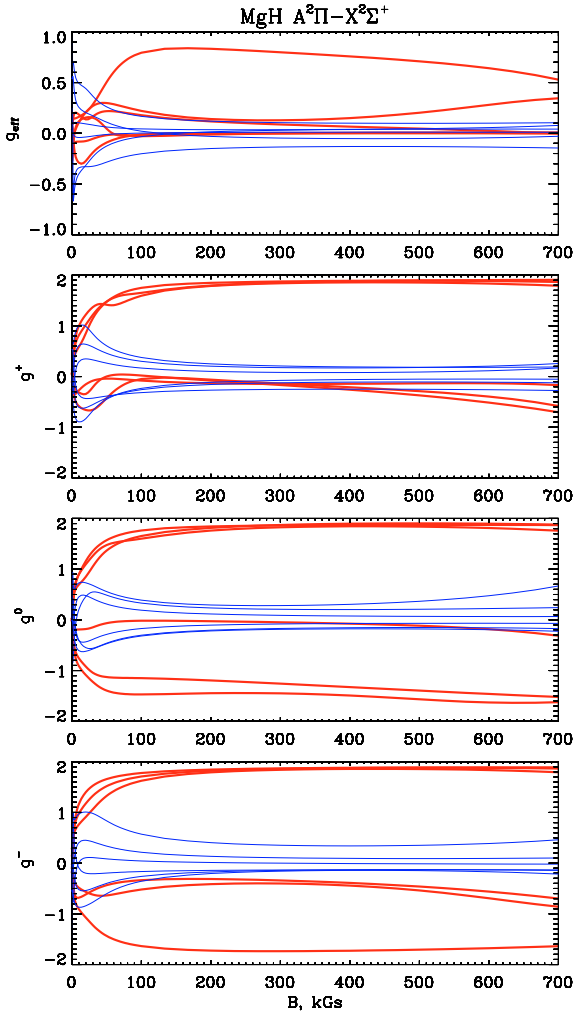

Fig. 7. The same as in Fig. 6 for $g_{\rm eff}$, g^+, g^0 and g^-. In the Zeeman regime Landé factors of the transitions are relatively small. As the magnetic field strength increases, all lines show significant magnetic sensitivity. Similar to the line strengths, the most rapid changes occur in the intermediate PBR. In the complete PBR on the fine structure the magnetic sensitivity is again reduced because of the symmetric splitting. In practice, when line strengths are combined with Landé factors, the satellite and forbidden transitions would dominate the polarisation signal in the complete PBR. Different behaviour of g^+, g^0 and g^- reflects the asymmetry in magnetic line patterns. Again, such a behaviour is typical for other electronic transitions.

PBR (0.1 and 1 kG), the upper state is in the intermediate PBR (10 kG) and both states are in the complete PBR (100 kG). Fading of the main branch lines and strengthening of the satellite branch lines are obvious. Note also, that in the intermediate PBR relative intensities of the σ^+ and σ^- of the main branch lines become very different. This results in a net polarisation signal in the lines which can be observed in both linear and circular polarisation.

When the molecular structure enters the PBR on the rotational structure, a great number of previously forbidden transitions with $|\Delta J| \geq 2$ and $|\Delta N| \geq 2$ appear in the spectrum. As the level structure becomes very much perturbed (Fig. 5) no transitions can be identified as belonging to main or satellite branches. According to the selection rule $\Delta M = 0, \pm 1$ the spectrum of the molecule would be a mixture of different transitions between M-sublevels. If one of the involved electronic states is a Σ-state, some grouping of the transitions according to a pseudo-multiplet structure (Fig. 4) is expected.

5.2. Stokes parameters

In order to calculate Stokes parameters of molecular transitions we employ the method of polarised radiative transfer described in Paper II. It is valid for both Zeeman and Paschen-Back regimes when the splitting pattern of a molecular line and the

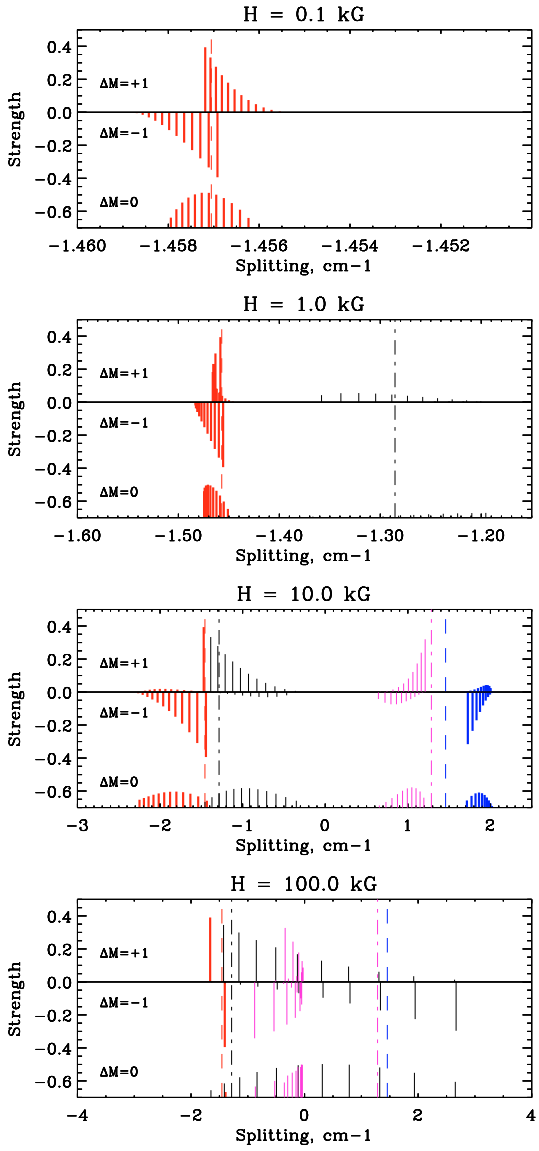

Fig. 8. Magnetic patterns for the $P_1 +^P Q_{12}$ and $P_2 +^P O_{21}$ transitions with $N'' = 6$ for different magnetic field strengths. The components with $\Delta M = -1$ are plotted downward for clarity. Vertical dashed and dashed-dotted lines indicate the positions of the main and satellite lines, respectively, at zero magnetic field. The components shown by thick and thin sticks correspond to the main and satellite lines, respectively. In the top plot only P_1 line is shown. For the field of 1 kG, P_1 is shown together with Q_{12}, which is very weak. Note that already at 1 kG the PBE is well seen in the P_1 line shape. The intensity and splitting of the satellite lines become comparable to and even exceed those of the main lines at fields of 10 kG and 100 kG. The $R_1 +^R S_{12}$ and $R_2 +^R Q_{21}$ transitions show similar patterns and behaviour but of opposite sign.

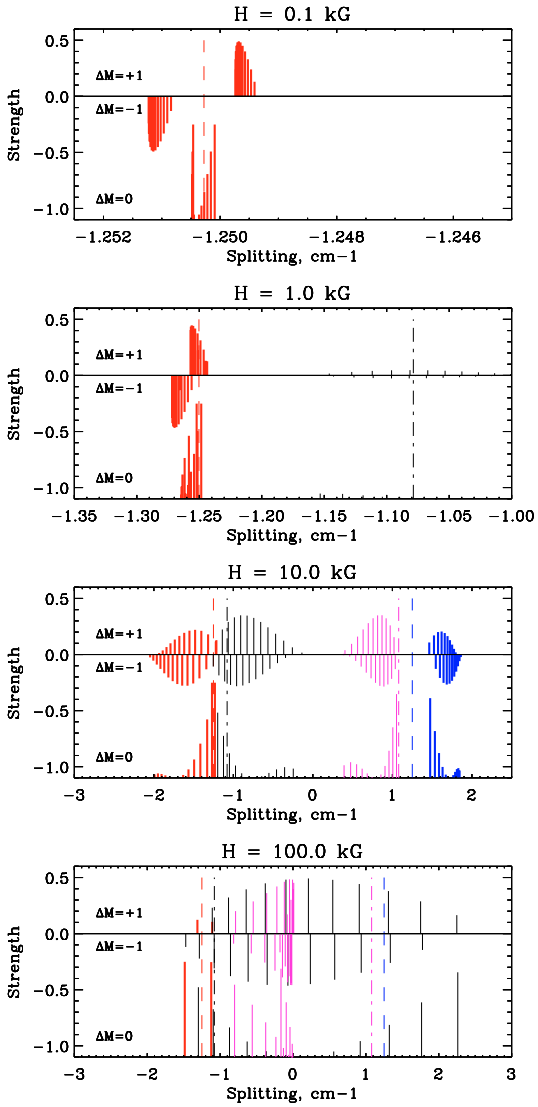

Fig. 9. The same as Fig. 8 for the $Q_1 +^Q R_{12}$ and $Q_2 +^Q P_{21}$ transitions with $N'' = 6$.

line absorption matrix are accordingly calculated. The code STOPRO (Solanki 1987; Frutiger et al. 2000) extended to include molecular transitions (Berdyugina et al. 2000, 2003) is used.

In Fig. 10 we present Stokes V profiles of the MgH A–X (0,0) $P_1 +^P Q_{12}$ and $P_2 +^P O_{21}$ transitions for N'' from 4 to 10 for a longitudinal magnetic field with a strength of 2 kG. The most striking feature is that all individual Stokes V profiles shown in the top plot are essentially single-lobed, which is the most prominent signature of the PBR. When Stokes V profiles of the main and satellite are calculated together, the profiles look more symmetrical for lower N numbers and become very asymmetric for higher N numbers. This occurs due to the rapid decrease of the magnetic sensitivity of the main branch lines with N (negative Stokes V in this example) combined with the slower change in the magnetic sensitivity of the satellite lines (here, positive Stokes V). Such a combination results in increasing the net circular polarisation signal with N in the beginning of the band. For larger N numbers, the signal goes to zero because of the reduced PBE at the same field strength. A similar behaviour is found for the $R_1 +^R S_{12}$ and $R_2 +^R Q_{21}$ transitions. Stokes V profiles for the $Q_1 +^Q R_{12}$ and $Q_2 +^Q P_{21}$ transitions are shown in Fig. 12. Here only satellite lines exhibit single-lobed profiles, while main branch lines maintain almost antisymmetric shapes, which are emphasised when pairs of lines are calculated together (bottom plot).

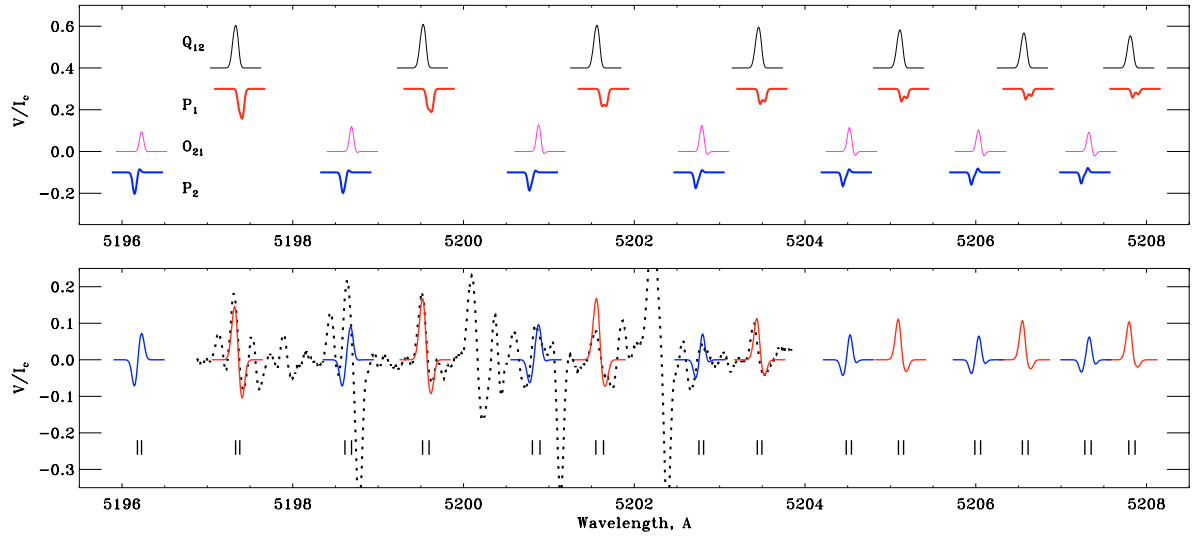

Fig. 10. Stokes V profiles of the MgH A–X (0,0) $P_1 +^P Q_{12}$ and $P_2 +^P O_{21}$ transitions for N'' from 4 to 10 (*left to right*) for the longitudinal magnetic field of 2 kG. In the top plot, profiles for individual lines are shown separately (shifted in the vertical scale for clarity). Note that all profiles are single-lobed already at this field strength. In the bottom plot, Stokes V profiles are calculated including all transitions simultaneously. Vertical dashes indicate the position of lines at zero magnetic field. The calculations are plotted on top of the Stokes V spectrum observed in a sunspot (dotted line, from Berdyugina et al. 2000).

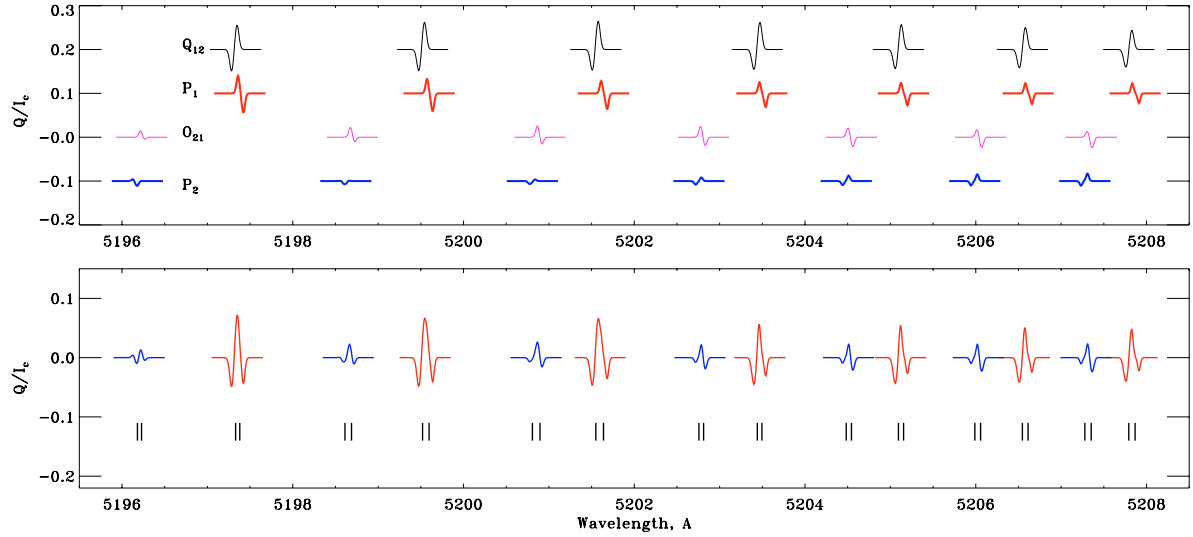

Fig. 11. Stokes Q profiles of the the same transitions as in Fig. 10 for a transversal magnetic field of 2 kG. Note that all individual profiles in the top plot have nearly antisymmetric shapes. When Stokes Q profiles of the main and satellite lines are calculated together, the resulting shape is reminiscent of a Stokes Q profile as would be observed in the Zeeman regime.

The dotted line in Fig. 10 represents observations made by W. Livingston in a sunspot umbra (see Berdyugina et al. 2000, for details). Obviously there is significant blending by other lines in the data. In order to use MgH line to diagnose sunspot and starspot magnetic fields, the blending lines will have to be included in the analysis. This will be the topic of a separate publication.

Stokes Q profiles in the transversal magnetic field for the $P_1 +^P Q_{12}$ and $P_2 +^P O_{21}$ transitions are shown in Fig. 11. Again, the individual line shapes are very different from what is normally observed in the Zeeman regime. Instead of being symmetric, the profiles are essentially antisymmetric and are more reminiscent of normal Stokes V profiles. The polarisation signal of satellite lines is larger than that of main branch lines, although the former are still weaker in Stokes I than the latter. Also, their sign of polarisation is opposite. Because of wavelength shifts between main and satellite lines, the resultant Stokes Q signal from pairs of lines look almost symmetric and very similar to that observed in the Zeeman regime. This visible symmetry is however very sensitive to the magnetic field strength. Stokes Q profiles for the $Q_1 +^Q R_{12}$ and $Q_2 +^Q P_{21}$ transitions are shown in Fig. 13. In this case the individual line profiles are intermediate between antisymmetric and single-lobed shapes. Again, the polarisation signal of satellite lines is larger and of opposite sign as compared to main branch lines. As a result, the polarisation pattern of line pairs

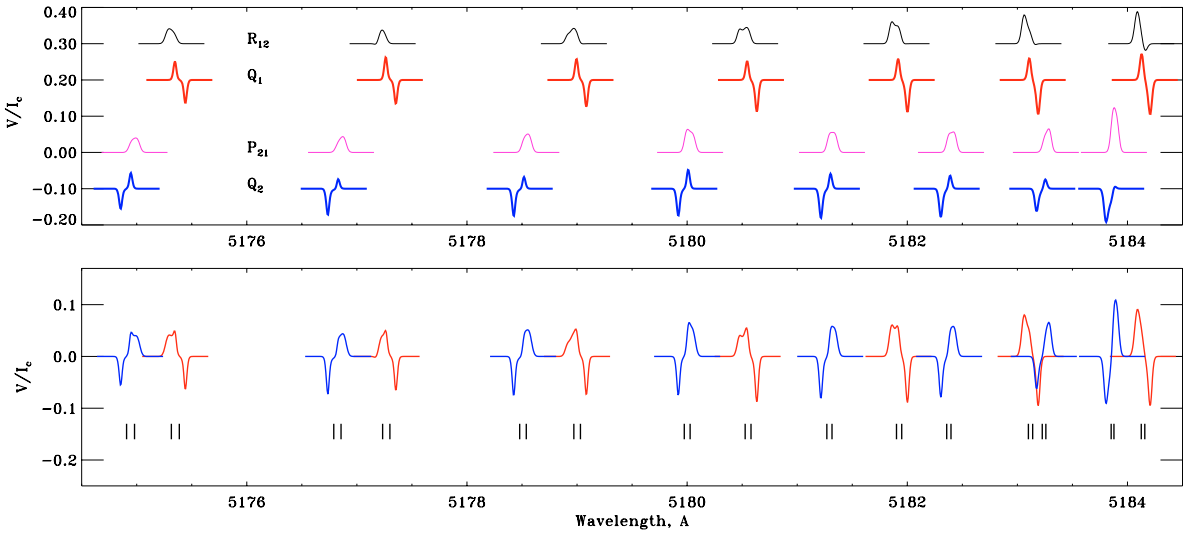

Fig. 12. The same as Fig. 10 for the $Q_1 +^Q R_{12}$ and $Q_2 +^Q P_{21}$ transitions with N'' from 10 to 4 (*left to right*).

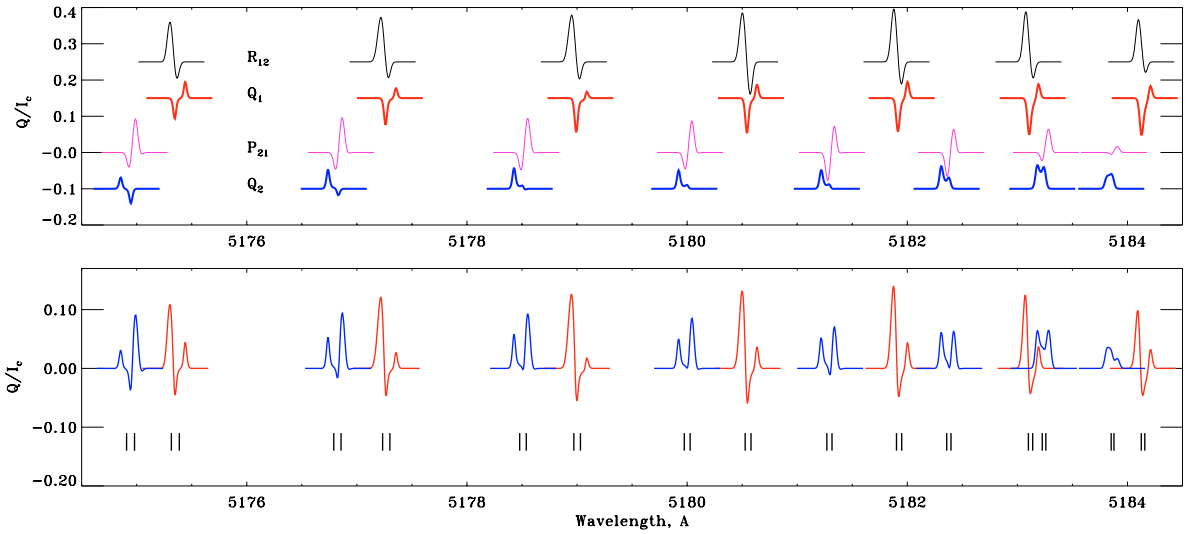

Fig. 13. The same as Fig. 11 for the $Q_1 +^Q R_{12}$ and $Q_2 +^Q P_{21}$ transitions with N'' from 10 to 4 (*left to right*).

is irregular and dominated by one polarisation sign, producing net linear polarisation over the whole wavelength interval.

These examples demonstrate clear advantages for studying both solar and stellar magnetic fields using molecular lines. In sunspots, the magnetic field strength can be diagnosed not only from the line splitting and amplitude of the polarisation signal as in the Zeeman regime but also from the analysis of line asymmetries for different N numbers. This is qualitatively new information which would strongly constrain the magnetic field in sunspots, in particular in the cooler parts of the umbra. For stars, the net polarisation signal would enable the detection of stellar magnetic fields even at moderate spectral resolution.

6. Discussion and conclusions

In the visible and infrared (IR) parts of the sunspot spectrum, lines of about a dozen diatomic molecules have been identified. In the visible and near IR they arise due to electronic-vibration-rotational transitions, while in the far IR and longer wavelengths the observed molecular transitions are either ro-vibrational or pure rotational. Many of these transitions and some others are observed in spectra of cool stars as well. In Table 1 we present a list of the transitions which would be observed in the PBR at typical sunspot and stellar magnetic field strengths. The magnetic field strength at which the PBE becomes significant is provided. In most cases the PBE occurs already at field strengths below a few hundreds Gs. This indicates the importance of the present theoretical study of the molecular PBE. For degenerate stars, having stronger fields, this list can be extended.

For the first time, we presented a self-consistent theoretical description of the molecular Paschen-Back effect for the Hund's case intermediate between (a) and (b), when the molecular total spin becomes partly uncoupled from the orbital momentum, internuclear axis and rotation. Depending on how strong the spin-orbital coupling is, the PBE occurs first

Table 1. Transitions of diatomic molecules in the optical and IR that are present in sunspot and stellar spectra in the PBR.

	Electronic transition	λ (Å)	$H^{(1)}$ (G)
OH	$A^2\Sigma - X^2\Pi$	2800–3400	2100
CN	$A^2\Pi - X^2\Sigma$	7350–11580	77
	$B^2\Sigma - X^2\Sigma$	3490–4215	77
MgH	$A^2\Pi - X^2\Sigma^+$	4780–5620	280
	$B'^2\Sigma^+ - X^2\Sigma^+$	5370–7590	280[(2)]
CaH	$A^2\Pi - X^2\Sigma^+$	6680–7590	470
	$B^2\Sigma^+ - X^2\Sigma^+$	6170–6870	148
CH	$A^2\Delta - X^2\Pi$	4150–4400	135[(3)]
	$B^2\Sigma^- - X^2\Pi$	3870–4120	305
	$C^2\Sigma^+ - X^2\Pi$	3080–3290	535
	$X^2\Pi$	32920–40330	135[(3)]
SH	$A^2\Sigma - X^2\Pi$	3250–3300	3350
NH	$A^3\Pi - X^3\Sigma^-$	3280–3470	970
	$X^3\Sigma^-$	28900–35720	970
VO	$A^4\Pi - X^4\Sigma^+$	10470–11970	240[(4)]
	$B^4\Pi - X^4\Sigma^+$[(5)]	7330–8060	240
	$C^4\Sigma^+ - X^4\Sigma^+$	5730–5760	240
CrH	$A^6\Sigma^+ - X^6\Sigma^+$	7000–9520	44

[(1)] The equivalent magnetic field strength is calculated for the smallest splitting in the state. It represents an estimate of the field strength at which the PBE becomes significant. [(2)] Fine structure of the upper state was not resolved. [(3)] Only some transitions are affected by the PBE. [(4)] The ground state of VO shows a relatively strong spin-spin interaction, so that the multiplet sublevels become quickly well separated in energy. [(5)] The upper state $B^4\Pi$ of the system is strongly perturbed by the nearby $a^2\Sigma^+$ state, so that a significant magnetic sensitivity is expected for this system.

either on the rotational structure (case a) or on the fine structure (case b) of the electronic term. As the field strength increases, both structures become strongly perturbed. In Σ-states, which are in pure Hund's case (b) because $\Lambda = 0$, the interaction between the spin and the rotation moment defines the fine structure of the electronic state. Therefore, the PBE occurs due to the spin decoupling from the rotation. We described a numerical approach to the problem of finding perturbed energy levels and transition probabilities in the PBR. Our approach is valid for terms of any multiplicity and can be used to calculate Stokes parameters of molecular transitions presented in Table 1 and many more. The approach can be further extended for partial uncoupling of the orbital momentum from the internuclear axis, when the transition to the Hund's case (d) occurs. This is the subject of a forthcoming investigation.

We introduced a generalised definition of effective magnetic Landé factors which can be employed when assuming the weak-field approximation in the Paschen-Back regime. It is also useful for studying variations of the polarisation properties of molecular transitions with magnetic field strengths. The new definition is fully compatible with the conventional one for the Zeeman regime. It can be also applied to the PBE of atomic lines.

To demonstrate the properties of the electronic states in the PBR, we calculated examples of magnetic splitting of molecular levels with different values of the total spin and orbital momentum in the PBR on both fine and rotational structures of the states. We also presented illustrative examples of the typical behaviour of molecular line strengths and polarisation patterns in the presence of strong magnetic fields. The calculated examples allow us to distinguish two regimes of the PBE, which should be present in other cases as well:

- One or both involved electronic states are in the intermediate PBR. In this case, the total spin is only partly uncoupled from other molecular momenta. Therefore, magnetic splitting and Stokes profiles are strongly asymmetric, and line strengths and profiles are very sensitive to the magnetic field. Forbidden and satellite transitions are comparable in strength with main branch transitions.
- Both states are in the complete PBE on the same structure (rotational or fine). In this case, the total spin is quantised independently on the field direction. Thus, magnetic splitting and Stokes profiles become symmetric and reminiscent of those in the Zeeman regime. Forbidden and satellite transitions are much stronger than main branch transitions.

This generalised description of the PBE on the molecular structure in cases intermediate between Hunds (a) and (b) implies a large variety of different cases and regimes when applied to particular electronic transitions, such as those listed in Table 1.

The presented calculations give a first indication of the remarkable potential of the molecular PBE for new diagnostics of solar and stellar magnetic fields. Here we calculated only one example of transitions observed in spectra of sunspots and cool stellar atmospheres which demonstrated typical pecularities of the polarisation signal in molecular lines in the PBR. The development of new diagnostic techniques based on these and other transitions listed in Table 1 would require the extensive and detailed examination of each electronic state and transition. With the present paper we now have the main tools at our disposal to carry out such an investigation.

Acknowledgements. We are thankful to N. Afram and A. Shapiro for their help in calculations. S. V. Berdyugina acknowledges the EURYI award from the ESF, the SNF grants PE002-104552 and 200021-103696, and the ETH Research Grant TH-2/04-3.

Appendix A: Matrix elements

Table A.1. Matrix elements of $\mathcal{H}_{\rm int}$ in Hund's case (a) wavefunctions, according to Kovàcs (1969).

$\mathcal{H}_{\rm SL}(\Lambda,\Sigma,J;\Lambda,\Sigma,J)$	$A\Lambda\Sigma$
$\mathcal{H}_{\rm rot}(\Lambda,\Sigma,J;\Lambda,\Sigma,J)$	$B[J(J+1)-\Omega^2+S(S+1)-\Sigma^2]$
$\mathcal{H}_{\rm rot}(\Lambda,\Sigma,J;\Lambda,\Sigma\pm1,J)$	$B\sqrt{S(S+1)-\Sigma(\Sigma\pm1)}\sqrt{J(J+1)-\Omega(\Omega\pm1)}$
$\mathcal{H}_{\rm c}(\Lambda,\Sigma,J;\Lambda,\Sigma\pm1,J)$	$-2D[J(J+1)-\Omega(\Omega\pm1)+S(S+1)-\Sigma(\Sigma\pm1)-1]$
	$-2D\sqrt{S(S+1)-\Sigma(\Sigma\pm1)}\sqrt{J(J+1)-\Omega(\Omega\pm1)}$
$\mathcal{H}_{\rm c}(\Lambda,\Sigma,J;\Lambda,\Sigma\pm2,J)$	$-D\sqrt{S(S+1)-\Sigma(\Sigma\pm1)}\sqrt{S(S+1)-(\Sigma\pm1)(\Sigma\pm2)}$
	$\sqrt{J(J+1)-\Omega(\Omega\pm1)}\sqrt{J(J+1)-(\Omega\pm1)(\Omega\pm2)}$
$\mathcal{H}_{\rm SR}(\Lambda,\Sigma,J;\Lambda,\Sigma,J)$	$\gamma[\Sigma^2-S(S+1)]$
$\mathcal{H}_{\rm SR}(\Lambda,\Sigma,J;\Lambda,\Sigma\pm1,J)$	$-\frac{1}{2}\gamma\sqrt{S(S+1)-\Sigma(\Sigma\pm1)}\sqrt{J(J+1)-\Omega(\Omega\pm1)}$
$\mathcal{H}_{\rm SS}(\Lambda,\Sigma,J;\Lambda,\Sigma,J)$	$\lambda[3\Sigma^2-S(S+1)]$

Table A.2. Matrix elements of $\mathcal{H}_{\rm int}$ in Hund's case (b) wavefunctions, according to Kovàcs (1969).

$\mathcal{H}_{\rm rot}(\Lambda,N;\Lambda,N)$	$B[N(N+1)-\Lambda^2]$
$\mathcal{H}_{\rm SL}(\Lambda,N;\Lambda,N)$	$A\frac{\Lambda^2}{2N(N+1)}[J(J+1)-N(N+1)-S(S+1)]$
$\mathcal{H}_{\rm SL}(\Lambda,N;\Lambda,N+1)$	$A\frac{\Lambda}{2(N+1)}\sqrt{(N+1)^2-\Lambda^2}\sqrt{(J+N+1)(J+N+2)-S(S+1)}\sqrt{\frac{S(S+1)-(J-N)(J-N-1)}{(2N+1)(2N+3)}}$
$\mathcal{H}_{\rm c}(\Lambda,N;\Lambda,N)$	$-D[N(N+1)-\Lambda^2]^2$
$\mathcal{H}_{\rm SR}(\Lambda,N;\Lambda,N)$	$\frac{1}{2}\gamma[J(J+1)-N(N+1)-S(S+1)][1-\frac{\Lambda^2}{N(N+1)}]$
$\mathcal{H}_{\rm SS}(\Lambda,N;\Lambda,N)$	$-2\lambda\frac{3/4\,C(C+1)-N(N+1)S(S+1)}{(2N-1)(2N+3)}[1-\frac{3\Lambda^2}{N(N+1)}]$, $C=J(J+1)-N(N+1)-S(S+1)$

Table A.3. Matrix elements of $\mathcal{H}_{\rm H}$ in Hund's case (a) wavefunctions, according to Schadee (1978) with the sign changed for those elements which are responsible for the interaction of levels with different spin projections, in order to match the sign convention for the spin operator by Kovàcs (1969).

$\mathcal{H}_{\rm H}(\Lambda,\Sigma,J,M;\Lambda,\Sigma,J,M)$	$\Delta\sigma_0\frac{\Lambda+2\Sigma}{J(J+1)}\Omega M$
$\mathcal{H}_{\rm H}(\Lambda,\Sigma,J,M;\Lambda,\Sigma\pm1,J,M)$	$-\Delta\sigma_0\frac{M}{J(J+1)}\sqrt{(J\mp\Omega)(J\pm\Omega+1)}\sqrt{(S\mp\Sigma)(S\pm\Sigma+1)}$
$\mathcal{H}_{\rm H}(\Lambda,\Sigma,J,M;\Lambda,\Sigma,J+1,M)$	$\Delta\sigma_0\frac{\Lambda+2\Sigma}{J+1}\sqrt{\frac{(J+\Omega+1)(J-\Omega+1)(J+M-1)(J-M+1)}{(2J+1)(2J+3)}}$
$\mathcal{H}_{\rm H}(\Lambda,\Sigma,J,M;\Lambda,\Sigma\pm1,J+1,M)$	$\pm\Delta\sigma_0\frac{1}{J+1}\sqrt{\frac{(J\pm\Omega+1)(J\pm\Omega+2)(J+M+1)(J-M+1)(S\mp\Sigma)(S\pm\Sigma+1)}{(2J+1)(2J+3)}}$
$\mathcal{H}_{\rm H}(\Lambda,\Sigma,J,M;\Lambda,\Sigma,J-1,M)$	$\Delta\sigma_0\frac{\Lambda+2\Sigma}{J}\sqrt{\frac{(J+\Omega)(J-\Omega)(J+M)(J-M)}{(2J-1)(2J+1)}}$
$\mathcal{H}_{\rm H}(\Lambda,\Sigma,J,M;\Lambda,\Sigma\pm1,J-1,M)$	$\mp\Delta\sigma_0\frac{1}{J}\sqrt{\frac{(J\mp\Omega)(J\mp\Omega-1)(J+M)(J-M)(S\mp\Sigma)(S\pm\Sigma+1)}{(2J-1)(2J+1)}}$

Table A.4. Matrix elements of $\mathcal{H}_{\rm H}$ in Hund's case (b) wavefunctions, according to Hill (1929).

$\mathcal{H}_{\rm H}(\Lambda,N,J,M;\Lambda,N,J,M)$	$\Delta\sigma_0\frac{M}{J(J+1)}\{J(J+1)+S(S+1)-N(N+1)$ $+\frac{\Lambda^2}{2N(N+1)}[J(J+1)+N(N+1)-S(S+1)]\}$
$\mathcal{H}_{\rm H}(\Lambda,N,J,M;\Lambda,N,J+1,M)$	$\Delta\sigma_0\frac{1}{J+1}\sqrt{\frac{(J+1)^2-M^2}{(2J+1)(2J+3)}}$ $\times\{\sqrt{(J+S+1)(J+S+2)-N(N+1)}\sqrt{N(N+1)-(J-S)(J-S+1)}$ $-\frac{\Lambda^2}{2N(N+1)}\sqrt{(J+N+1)(J+N+2)-S(S+1)}\sqrt{S(S+1)-(J-N)(J-N+1)}\}$
$\mathcal{H}_{\rm H}(\Lambda,N,J,M;\Lambda,N+1,J,M)$	$\Delta\sigma_0\frac{M}{J(J+1)}\frac{\Lambda}{2(N+1)}\sqrt{(N+1)^2-\Lambda^2}\sqrt{(J+N+1)(J+N+2)-S(S+1)}$ $\times\sqrt{\frac{S(S+1)-(J-N)(J-N-1)}{(2N+1)(2N+3)}}$
$\mathcal{H}_{\rm H}(\Lambda,N,J,M;\Lambda,N+1,J+1,M)$	$\Delta\sigma_0\frac{1}{J(J+1)}\frac{\Lambda}{2(N+1)}\sqrt{\frac{[(N+1)^2-\Lambda^2][(J+N+1)(J+N+2)-S(S+1)]}{(2N+1)(2N+3)}}$ $\times\sqrt{\frac{[(J+1)^2-M^2][(J+N+2)(J+N+3)-S(S+1)]}{(2J+1)(2J+3)}}$
$\mathcal{H}_{\rm H}(\Lambda,N,J,M;\Lambda,N+1,J-1,M)$	$-\Delta\sigma_0\frac{1}{J}\frac{\Lambda}{2(N+1)}\sqrt{\frac{[(N+1)^2-\Lambda^2][S(S+1)-(J-N-1)(J-N)]}{(2N+1)(2N+3)}}$ $\times\sqrt{\frac{[J^2-M^2][S(S+1)-(J-N-2)(J-N-1)]}{(2J-1)(2J+1)}}$

References

Asensio Ramos, A., Trujillo Bueno, J., Bianda, M., Manso Sainz, R., & Uitenbroek, H. 2004, ApJ, 611, L61

Asensio Ramos, A., Trujillo Bueno, J., & Collados, M. 2005, ApJ, 623, L57

Berdyugina, S. V., & Solanki, S. K. 2001, A&A, 380, L5

Berdyugina, S. V., & Solanki, S. K. 2002, A&A, 385, 701 (Paper I)

Berdyugina, S. V., Frutiger, C., Solanki, S. K., & Livingston, W. 2000, A&A, 364, L101

Berdyugina, S. V., Solanki, S. K., & Frutiger, C. 2001, in Magnetic Fields across the Herzsprung-Russel Diagram, ed. G. Mathys, S. K. Solanki, & D. T. Wickramasinghe, ASP Conf. Ser.

Berdyugina, S. V., Stenflo, J. O., & Gandorfer, A. 2002, A&A, 388, 1062

Berdyugina, S. V., Solanki, S. K., & Frutiger, C. 2003, A&A, 412, 513 (Paper II)

Frutiger, C., Solanki, S. K., Fligge, M., & Bruls, J. H. M. J. 2000, A&A, 358, 1109

Herzberg, G. 1950, Molecular Spectra and Molecular Structure. I. Spectra of Diatomic Molecules (New York: Van Nostrand Company)

Hill, E. L. 1929, Phys. Rev., 34, 1507

Hougen, J. T. 1970, The calculation of rotational energy levels and rotational line intensities in diatomic molecules, NBS Mon., 115

Illing, R. M. E. 1981, ApJ, 248, 358

Kovàcs, I. 1969, Rotational Structure in the Spectra of Diatomic Molecules (London: Adam Hilger Ltd.)

Schadee, A. 1978, JQSRT, 19, 517

Solanki, S. K. 1987, Ph.D. Thesis, ETH, Zürich

Uitenbroek, H., Miller-Ricci, E., Asensio Ramos, A., & Trujillo Bueno, J. 2004, ApJ, 604, 960